Lasers Manuf. Mater. Process. (2016) 3:111–130
DOI 10.1007/s40516-016-0024-9

Laser Non-Uniform Heating of Moving Thin Wires Below the Biot Number Criterion of Uniform Temperature

Thiwanka Wickramasooriya[1,2,3] · **Raj Vaidyanathan**[3] · **Aravinda Kar**[1]

Accepted: 20 January 2016 / Published online: 5 February 2016

Abstract An analytic solution is obtained for three-dimensional quasi-steady state temperature distribution during laser heating of moving thin wires. The wire moves at a constant speed through a vacuum chamber, which is back-filled with an inert gas such as argon, and a laser beam of rectangular cross-section is incident on the wire. The ambient gas provides a convection heat transfer mechanism, which yields a Biot number, Bi, for the heating process to determine whether the temperature distribution would be uniform or nonuniform in the cross-section of the wire. Generally, the criterion of Bi less than 0.1 is applied to assume spatially uniform temperature distribution in a solid. The temperature distribution is determined for different Bi numbers and the variation of the temperature in the azimuthal direction is analyzed. The method of solution involves the Fourier transform in the azimuthal direction and the Hankel transform in the radial direction for a three-dimensional quasi-steady state heat conduction equation containing an advection term that accounts for the motion of the wire. The thermal and optical properties of the material is assumed to be constant in the temperature range of this study. The heat loss due to radiation heat transfer between the wire surface and the surrounding environment is neglected due to the small laser-heated surface area. Using this model, the temperature profile is studied for different process parameters such as the incident laser power, laser beam profile, Biot number, and wire speed.

✉ Aravinda Kar
akar@creol.ucf.edu

[1] Laser-Advanced Materials Processing Laboratory, CREOL, The College of Optics and Photonics, University of Central Florida, Orlando, FL 32816-2700, USA

[2] Mechanical and Aerospace Engineering Department, University of Central Florida, Orlando, FL 32816-2700, USA

[3] Materials Science and Engineering Department, Advanced Materials Processing and Analysis Center, University of Central Florida, Orlando, FL 32816-2700, USA

Keywords Laser heating · Thin wire · 3-dimentional heat conduction · Integral transformation

Introduction

The capability of lasers for localized heating with high precision has been widely used in numerous applications such as laser cutting, welding, drilling and cladding, among others. It is, however, evident from the available literature that very little work has been done on the laser surface modification of thin wires, such as the deposition of thin or nanoscale films by laser chemical vapor deposition, laser diffusion of trace elements into the wire from organometallic precursors, or interfacial composition modification by laser heat treatment of coated thin wires. Surface modified thin wires have potential as medical implants, such as pacemaker leads, neurostimulators and dentals braces, for which the wires must be biocompatible and not heat up due to the radio-frequency magnetic field during magnetic resonance imaging. Chen, Vaidyanathan and Kar [1–3] incorporated a trace of Pt into thin sheets of Ti and Ta by a laser diffusion process and demonstrated heating reduction in a time-varying magnetic field. A fundamental understanding of the laser heating of thin wires is necessary to analyze the effect of different process parameters on the azimuthal variation of the temperature distribution for modifying the wire surface uniformly over the entire circumference.

To estimate the laser process parameters for experimental studies or manufacturing applications, it is essential to have a theoretical model of the process [4–7], because the model can reduce the time required to optimize and scale up the process, and for developing efficient process control and monitoring systems. Laser heating of a substrate involves several phenomena, such as heat conduction, melting, convection, vaporization and plasma formation, depending on the applications [8–10]. Yilbas and Al-Dweik [11] presented an analytic solution for short-pulse laser heating of semi infinitely long, microsize, e.g., 2 μm diameter, stationary wires for the case of laser irradiance over the entire cross section of the wire. They used a modified heat conduction equation to account for the thermal separation of electron and lattice subsystems that occur during short-pulse laser heating. The laser irradiation is usually considered to be perpendicular to the substrate surface [12–14], which would be a reasonable approximation even when the laser beam is incident on the curved surface of a cylinder provided the diameter of the cylinder is much larger than the laser beam diameter. In the present study, the laser beam is incident on the cylindrical surface of a moving thin wire of diameter comparable to the size of the laser beam and, therefore, the incident angle between the laser beam and the wire surface is a function of position. The laser beam is incident on the upper half of the wire surface and the corresponding heat flux is limited only to the top portion of the wire. Under this laser heating condition, the wire temperature profile is obtained by using the Fourier heat conduction equation.

Laser-Wire Interaction and Heating Model

A Gaussian laser beam is incident on a thin wire in the negative y′ direction as shown in Fig. 1 and the beam is normal to the surface only at the top most points along the z′

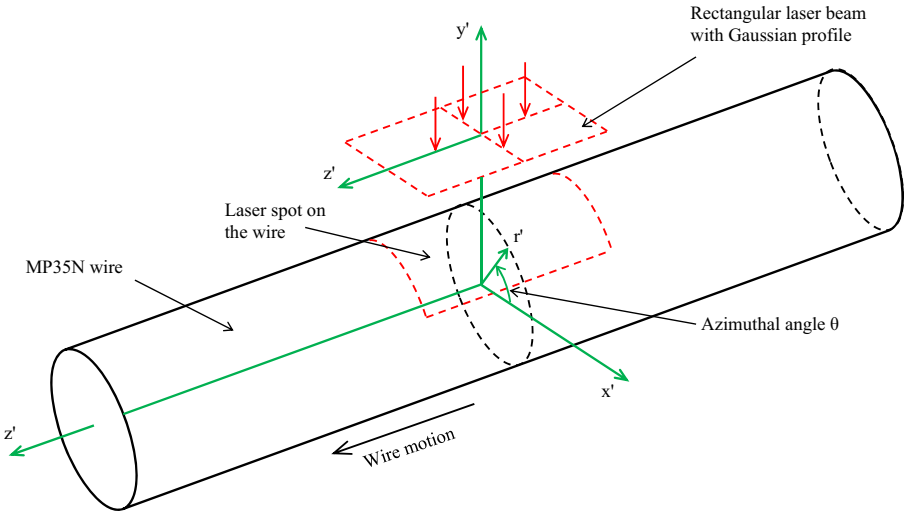

Fig. 1 Laser heating of a moving wire and relevant coordinate system (color only in online version – Created using MS Word)

axis. The angle of incidence is oblique elsewhere as shown in Fig. 2. The heat flux to the wire surface is determined using the perpendicular component of the laser irradiation at all points of the surface. Hence the reflectivity can be considered to be constant equal to the reflectivity at normal incidence. The radius of the wire, which is made of a biocompatible material, MP35N, is $r_0' = 50\ \mu m$ in this study and its thermal conductivity varies from 11.5 to 23.4 W/m K at the temperature range of 21 to 649 °C, respectively [15]. This wire moves through a vacuum chamber that is filled with an inert gas argon and the wire is irradiated with a rectangular laser beam of length and

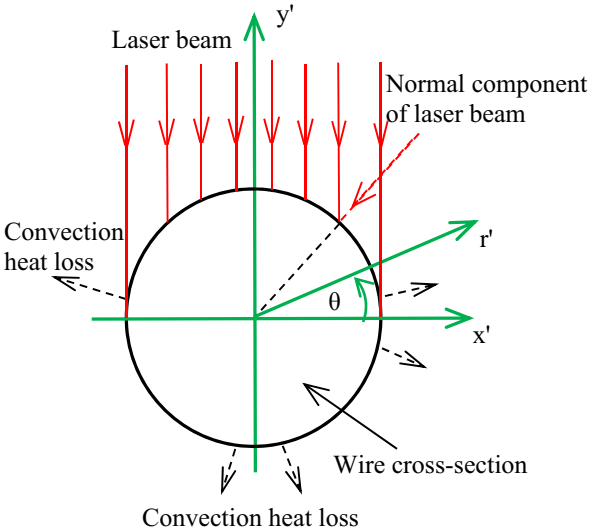

Fig. 2 Laser irradiation on wire cross-section of wire (color only in online version - Created using MS Word)

width 500 and 50 μm, respectively, on a plane tangential to the upper most point of the wire. The thermal conductivity is taken as 11.5 W/m K in this study.

The laser-heated spot on the moving wire creates localized convection in the argon gas, and the convection heat transfer coefficient is taken as $h = 250$ W/m^2 K that corresponds to the upper limit of the forced convection heat transfer coefficient in gases [16]. Two other convection heat transfer coefficients of 621 and 1242 W/m^2 K are also considered in this study to simulate laser heating of wires under liquid cooling conditions. Higher cooling rates can be achieved by fully or partially submerging the wire in a liquid because the forced convection heat transfer coefficient in liquids generally varies from 20 to 20 kW/m^2 K [16]. Laser heating of partially submerged wires can produce dissimilar properties in the liquid-cooled and gas-cooled regions due to differential cooling rates. This type of heating can be utilized to synthesize new materials with dissimilar properties across the cross section. Other applications of liquid cooling involve underwater laser materials processing such as underwater laser-assisted welding, cleaning, shock processing, cutting, surface hardening and residual stress relief in metal surfaces [17–20]. The convection around the wire generates a heat loss mechanism based on the Biot number, i.e., $Bi = hr_0'/k$, which is 0.0011 for the typical thermal conductivity of $k = 11.5$ and $h = 250$ W/m^2 K. Bi is an important metric for determining whether the temperature distribution would be spatially uniform in a solid. If Bi < 0.1, the error associated with assuming uniform temperature distribution is small [16].

The results of this study, however, show that the temperature distribution is significantly non-uniform in the cross-section of the thin wire even though the Bi is much lower than the limit of the Biot number criterion. Understanding the temperature profile across the thin section is important in microscale laser processing of materials, such as biomedical implants and microelectronic devises, and manufacturing of microscale and nanoscale structures. Establishing a uniform temperature profile is, particularly, critical when the effect around thin wires subsequent to laser heating depends on the temperature. For example, non-uniform temperature profiles can affect the uniformity of laser diffusion of a trace of elements or the thickness of nanoscale films deposited by the laser chemical vapor deposition process. Also the temperature gradients due to non-uniform temperature profiles would generate thermal stresses that can cause peeling of thin films, thermal distortion, cracks and breakage. These deleterious effects can be avoided by analyzing the temperature distribution in thin sections with an appropriate mathematical model.

A mathematical model is developed by considering a very long wire moving at a constant speed from a feeder spool to a take-up spool through an argon-filled chamber during laser heating of the wire as shown in Fig. 1. This is a time-dependent heat conduction problem due to the motion of the wire in the longitudinal direction. A short time after the initiation of the laser irradiation, however, the temperature distribution attains a steady state in a moving frame of reference fixed at the laser beam. In this frame of reference, the wire is considered to be infinitely long along the z′ coordinate axis and the wire moves in the z′ direction at a constant velocity U. The laser heating of the wire can be modelled as a quasi-steady state problem with an advection term in the conduction equation to account for the effect of U.

When the laser beam is incident on the wire, a part of the incident energy is reflected from the surface and the rest of the energy is absorbed within the laser-matter interaction volume inside the wire. However, the optical absorption depth of typical metals is 10–20 nm for the Nd:YAG laser of wavelength 1.06 μm [21, 22]. Therefore, the volumetric

heating effect of the laser can be neglected when the diameter of the metallic wire is much larger than the optical absorption depth. Typical metals reflect more than 90 % of the incident lasers of near infrared wavelengths such as a Nd:YAG laser of wavelength 1064 nm. The absorbed energy is transformed into heat due to the interaction between the photons and the electrons of the surface atoms of the wire, resulting in the generation of phonons. The heat is transferred from the surface to the rest of the wire by a three-dimensional heat conduction process. As the laser-heated spot moves away from the laser beam, the wire cools down due to convection heat transfer to the argon gas and radiative losses to the surrounding. Since the surface area of the laser-heated spot is very small, the radiation heat loss is considered to be small compared to the convection loss and the conduction through the wire and, therefore, the effect of radiation heat transfer is neglected in this study. Under these conditions, the laser heating of the wire is analyzed by considering three-dimensional quasi-steady state heat conduction in a moving frame of reference with a set of boundary conditions as given below:

$$\frac{\partial^2 T'}{\partial r'^2}+\frac{1}{r'}\frac{\partial T'}{\partial r'}+\frac{1}{r'^2}\frac{\partial^2 T'}{\partial \theta^2}-\frac{U}{\alpha}\frac{\partial T'}{\partial z'}+\frac{\partial^2 T'}{\partial z'^2}=0 \tag{1}$$

where T′ is the temperature of the wire at any radial (r′), azimuthal (θ) and axial (z′) location, and α is the thermal diffusivity of the wire. During the laser processing, the wire is fed to the laser beam from a feeding spool and wound onto a take up spool. Since these two spools are far away from the laser beam and the length of the laser spot is small, the wire is considered as an infinitely long moving cylinder.

The boundary conditions are:

$$T'|_{z'=\pm\infty}=T_\infty \tag{2}$$

$$-k\left.\frac{\partial T'}{\partial r'}\right|_{r'=r'_0}=\begin{cases}-I\left(x',z'\right)sin\theta+h\left[T'\left(r'_0,\theta,z'\right)-T_\infty\right] & 0\le\theta\le\pi\\ h\left[T'\left(r'_0,\theta,z'\right)-T_\infty\right] & \pi\le\theta\le 2\pi\end{cases} \tag{3}$$

At the cross section of the wire, where θ varies from 0 to 2π, the continuity of temperature and heat flux at any point yields the following two conditions in the θ direction.

$$T'|_{\theta=0}=T'|_{\theta=2\pi} \tag{4}$$

$$\left.\frac{\partial T'}{\partial \theta}\right|_{\theta=0}=\left.\frac{\partial T'}{\partial \theta}\right|_{\theta=2\pi} \tag{5}$$

where k is the thermal conductivity of the wire, h is the convection heat transfer coefficient and T_∞ is the temperature of the ambient argon gas far away from the

laser-heated spot. The absorbed energy flux supplied by the incident Gaussian laser intensity profile of rectangular cross-section is denoted by I(x′, z′) in boundary condition (3) where I(x′, z′)sinθ represents the heat flux normal to the wire surface, and I(x′, z′) is given by

$$I\left(x^{'},z^{'}\right)=I_0e^{-\left(\frac{2x^{'2}}{w_{x^{'}}^2}+\frac{2z^{'2}}{w_{z^{'}}^2}\right)} \tag{6}$$

where I_0 is a constant, and $w_{x'}$ and $w_{z'}$ are the half-length and half-width of the focused laser spot in the x′ and z′ directions, respectively, as shown in Fig. 2. I_0 is determined by conserving the absorbed laser energy, i.e.,

$$(1-R)P_i=I_0\int_{-\infty}^{\infty}e^{-\left(\frac{2x^{'2}}{w_{x^{'}}^2}\right)}\int_{-\infty}^{\infty}e^{-\left(\frac{2z^{'2}}{w_{z^{'}}^2}\right)}dx^{'}dz^{'} \tag{7}$$

where R is the reflectivity of the wire surface and P_i is the incident laser power, which yields

$$I_0=\frac{2(1-R)P_i}{\pi w_{x^{'}}w_{z^{'}}} \tag{8}$$

The above equations are non-dimensionalized by defining the following dimensionless variables:

$$z=\frac{z^{'}}{w_{z^{'}}},\qquad r=\frac{r^{'}}{r_0^{'}},\qquad T=\frac{T^{'}-T_\infty}{T_m} \tag{9}$$

where T_m is the melting temperature of the wire. So Eq. (1) can be written as

$$\frac{\partial^2T}{\partial r^2}+\frac{1}{r}\frac{\partial T}{\partial r}+\frac{1}{r^2}\frac{\partial^2T}{\partial\theta^2}-Pea_z\frac{\partial T}{\partial z}+a_z^2\frac{\partial^2T}{\partial z^2}=0 \tag{10}$$

where $a_z=r_0^{'}/w_{z'}$ and the Peclet number $Pe=Ur_0^{'}/\alpha$. The boundary conditions (2)–(5) can be written as follows in terms of the dimensionless variables:

$$T|_{z=\pm\infty}=0 \tag{11}$$

$$\left.\frac{\partial T}{\partial r}\right|_{r=1}+BiT|_{r=1}=\delta_\theta P_ae^{-2z^2}e^{-2a_x^2cos^2\theta}sin\theta \tag{12}$$

where $\delta_\theta=\begin{cases}1 & 0\le\theta\le\pi\\ 0 & \pi\le\theta\le2\pi\end{cases}$

$$T|_{\theta=0}=T|_{\theta=2\pi} \tag{13}$$

$$\left.\frac{\partial T}{\partial \theta}\right|_{\theta=0} = \left.\frac{\partial T}{\partial \theta}\right|_{\theta=2\pi} \tag{14}$$

where $a_x = r_0'/w_{x'}$ and $P_a = \frac{2P_i r_0'(1-R)}{\pi k T_m w_{x'} w_{z'}}$

Method of Solution

Equation (10) is solved by defining a new variable ψ(r,θ,z) for the temperature distribution T(r,θ,z) to eliminate the advection term ∂T/∂z. Representing the temperature variation in the azimuthal direction as a Fourier series and applying the Hankel transform in the radial direction, a second order ordinary differential equation is obtained which is solved by the method of variation of parameters. Expressing T in terms of ψ as follows

$$T = e^{\frac{Pe}{2a_z}z}\psi(r,\theta,z) \tag{15}$$

Equation (10) can be written as

$$\frac{\partial^2\psi}{\partial r^2} + \frac{1}{r}\frac{\partial\psi}{\partial r} + \frac{1}{r^2}\frac{\partial^2\psi}{\partial\theta^2} - \frac{Pe^2}{4}\psi + a_z^2\frac{\partial^2\psi}{\partial z^2} = 0 \tag{16}$$

and the boundary conditions (11–14) can be expressed as

$$\psi|_{z=\pm\infty} = 0 \tag{17}$$

$$\left.\frac{\partial\psi}{\partial r}\right|_{r=1} + Bi\psi|_{r=1} = \delta_\theta P_a e^{-\frac{Pe}{2a_z}z} e^{-2z^2} e^{-2a_x^2\cos^2\theta}\sin\theta \tag{18}$$

$$\psi|_{\theta=0} = \psi|_{\theta=2\pi} \tag{19}$$

$$\left.\frac{\partial\psi}{\partial\theta}\right|_{\theta=0} = \left.\frac{\partial\psi}{\partial\theta}\right|_{\theta=2\pi} \tag{20}$$

To solve Eq. (17), the Fourier series expansion of ψ yields

$$\psi = \sum_{m=0}^{\infty} T_{cm}\cos(m\theta) + \sum_{m=1}^{\infty} T_{sm}\sin(m\theta) \tag{21}$$

where $T_{cm}(r,m,z)$ and $T_{sm}(r,m,z)$ are coefficients of the series expansion, and ψ satisfies the boundary conditions (17–20). Substituting Eqs. (22) into (17) and equating

the coefficients of cos(mθ) ans sin(mθ) to zero, the equations T_{cm} and T_{sm} can be written as

$$\frac{\partial^2 T_{cm}}{\partial r^2}+\frac{1}{r}\frac{\partial T_{cm}}{\partial r}-\frac{m^2}{r^2}T_{cm}-\frac{Pe^2}{4}T_{cm}+a_z^2\frac{\partial^2 T_{cm}}{\partial z^2}=0 \tag{22}$$

$$\frac{\partial^2 T_{sm}}{\partial r^2}+\frac{1}{r}\frac{\partial T_{sm}}{\partial r}-\frac{m^2}{r^2}T_{sm}-\frac{Pe^2}{4}T_{sm}+a_z^2\frac{\partial^2 T_{sm}}{\partial z^2}=0 \tag{23}$$

which satisfy the following boundary conditions:

$$T_{cm}\big|_{z=\pm\infty}=0 \tag{24}$$

$$T_{sm}\big|_{z=\pm\infty}=0 \tag{25}$$

$$\sum_{m=0}^{\infty}\frac{\partial T_{cm}}{\partial r}\bigg|_{r=1}cos(m\theta)+Bi\sum_{m=0}^{\infty}T_{cm}\bigg|_{r=1}cos(m\theta)+\sum_{m=1}^{\infty}\frac{\partial T_{sm}}{\partial r}\bigg|_{r=1}sin(m\theta)+Bi\sum_{m=1}^{\infty}T_{sm}\bigg|_{r=1}sin(m\theta)=\delta_\theta P_a e^{-\frac{Pe}{2a_z}z}e^{-2z^2}e^{-2a_x^2cos^2\theta}sin\theta \tag{26}$$

The boundary conditions for T_{cm} and T_{sm} are separated by multiplying both sides of boundary condition (27) by cos(nθ) and sin(nθ), respectively, integrating with respect to θ from 0 to 2π and applying the orthogonality condition, which yield

$$\frac{\partial T_{cm}}{\partial r}\bigg|_{r=1}+BiT_{cm}|_{r=1}=\frac{P_a}{N_\theta}e^{-\frac{Pe}{2a_z}z}e^{-2z^2}\int_0^{\pi}e^{-2a_x^2cos^2\theta}sin\theta\cos(m\theta)d\theta \tag{27}$$

$$\frac{\partial T_{sm}}{\partial r}\bigg|_{r=1}+BiT_{sm}|_{r=1}=\frac{P_a}{N_\theta}e^{-\frac{Pe}{2a_z}z}e^{-2z^2}\int_0^{\pi}e^{-2a_x^2cos^2\theta}sin\theta\, sin(m\theta)d\theta \tag{28}$$

where, $N_\theta=\begin{cases}2\pi & m=0\\ \pi & m\neq 0\end{cases}$

The integrals in boundary conditions (28) and (29) can be evaluated by noting that $2\cos^2\theta = 1+\cos(2\theta)$ and using the following identity [23] in terms of the modified Bessel function of order k, $k = 0, 1, 2, \ldots$

$$e^{zcos\theta}=I_0(z)+2\sum_{k=1}^{\infty}I_k(z)cos\theta \tag{29}$$

So the integrals can be written as

$$\int_0^{\pi} e^{-2a_x^2\cos^2\theta}\sin\theta\cos(m\theta)d\theta = S_{cm} = \begin{cases} e^{-a_x^2}I_0\left(-a_x^2\right)\left[\frac{2}{1-m^2}\right] + e^{-a_x^2}\sum_{k=1}^{\infty} I_k\left(-a_x^2\right)\left[\frac{2(m-1)}{4k^2-(m-1)^2} - \frac{2(m+1)}{4k^2-(m+1)^2}\right] & m \text{ even} \\ 0 & else \end{cases} \tag{30}$$

$$\int_0^{\pi} e^{-2a_x^2\cos^2\theta}\sin\theta\sin(m\theta)d\theta = S_{sm} = \begin{cases} \frac{\pi}{2}e^{-a_x^2}\left[I_{\frac{m-1}{2}}\left(-a_x^2\right) - I_{\frac{m+1}{2}}\left(-a_x^2\right)\right] & m \text{ odd} \\ 0 & else \end{cases} \tag{31}$$

To transform boundary condition (28) into a homogeneous boundary condition, $T_{cm}(r,m,z)$ is written as a combination of three functions as given below.

$$T_{cm}(r,m,z) = F_{cm}(r,m,z) + f_{cm}(r,m)g_{cm}(z,m) \tag{32}$$

Equation (34) is substituted into Eq. (23) and the resulting expression yields the following two equations for F_{cm} and f_{cm}.

$$\frac{\partial^2 F_{cm}}{\partial r^2} + \frac{1}{r}\frac{\partial F_{cm}}{\partial r} - \left[\frac{m^2}{r^2} + \frac{Pe^2}{4}\right]F_{cm} + a_z^2\frac{\partial^2 F_{cm}}{\partial z^2} + a_z^2 f_{cm}\frac{\partial^2 g_{cm}}{\partial z^2} = 0 \tag{33}$$

and

$$\frac{\partial^2 f_{cm}}{\partial r^2} + \frac{1}{r}\frac{\partial f_{cm}}{\partial r} - \left[\frac{m^2}{r^2} + \frac{Pe^2}{4}\right]f_{cm} = 0 \tag{34}$$

Equation (34) is also substituted into Eq. (28) to obtain the following boundary conditions at $r = 1$.

$$\frac{\partial F_{cm}}{\partial r} + BiF_{cm} = 0 \tag{35}$$

$$g_{cm}\left[\frac{\partial f_{cm}}{\partial r} + Bif_{cm}\right]\Big|_{r=1} = \frac{P_a S_{cm}}{N_\theta}e^{-\frac{Pe}{2a_z}z}e^{-2z^2} \tag{36}$$

Equation (36) is Bessel's modified differential equation, which has a solution involving the modified Bessel functions of the first and second kinds $I_m(Pe\ r/2)$ and $K_m(Pe\ r/2)$, respectively, of order m. Since the temperature must be finite at $r = 0$ and

K_m is infinite at $r = 0$, K_m does not represent a physical solution to Eq. (36). Therefore, the solution is represented by

$$f_{cm} = C_1 I_m\left(\frac{Pe}{2}r\right) \tag{37}$$

where C_1 is an unknown constant. Substituting Eqs. (39) into (38), g_{cm} as determined as

$$g_{cm} = \frac{P_a S_{cm}}{N_\theta C_1\left[(m+Bi)I_m\left(\frac{Pe}{2}\right)+\frac{Pe}{2}I_m\left(\frac{Pe}{2}\right)\right]} e^{-\frac{Pe}{2a_z}z} e^{-2z^2} \tag{38}$$

Since the products $f_{cm}g_{cm}$ and $f_{cm}\frac{\partial^2 g_{cm}}{\partial z^2}$ in Eqs. (34) and (35), respectively, eliminates C_1 as can be seen from Eqs. (39) and (40), there is no need to determine C_1.

Applying the following Hankel transform [24] to Eq. (35),

$$\overline{F}_{cm}(\lambda_n, m, z) = \int_0^1 r J_m(\lambda_n r) F_{cm}(r, m, z) dr \tag{39}$$

the following equation is obtained for the transformed variable $\overline{F}_{cm}(\lambda_n, m, z)$,

$$\lambda_n^2 \overline{F}_{cm} - \frac{Pe^2}{4}\overline{F}_{cm} + {a_z}^2 \frac{\partial^2 \overline{F}_{cm}}{\partial z^2} + {a_z}^2 \frac{\partial^2 g_{cm}}{\partial z^2} C_1 \int_0^1 r J_m(\lambda_n r) I_m\left(\frac{Pe}{2}r\right) dr = 0 \tag{40}$$

and the associated boundary conditions are

$$\left.\overline{F}_{cm}\right|_{z=\pm\infty} = 0 \tag{41}$$

The eigenfunction $J_n(\lambda_n r)$ satisfies boundary condition (34) and yields the following equation [24] for the eigenvalues λ_n, $n = 0,1,2,3,.....$

$$\lambda_n[J_{m-1}(\lambda_n) - J_{m+1}(\lambda_n)] + BiJ_m(\lambda_n) = 0 \tag{42}$$

The term $\frac{\partial^2 g_{cm}}{\partial z^2}$, which can be determined from Eq. (37), and the integral in Eq. (39) are given by

$$\frac{\partial^2 g_{cm}}{\partial z^2} = \frac{P_a S_{cm}}{N_\theta\left[(m+Bi)I_m\left(\frac{Pe}{2}\right)+\frac{Pe}{2}I_m\left(\frac{Pe}{2}\right)\right]}\left[\left(\frac{Pe}{2a_z}+4z\right)^2 - 4\right] e^{-\frac{Pe}{2a_z}z} e^{-2z^2} \tag{43}$$

and

$$\int_0^1 r J_m(\lambda_n r) I_m\left(\frac{Pe}{2}r\right) dr = \frac{\lambda_n J_{m+1}(\lambda_n) I_m\left(\frac{Pe}{2}\right) - \frac{Pe}{2} J_m(\lambda_n) I_{m+1}\left(\frac{Pe}{2}\right)}{\lambda_n^2 - \frac{Pe^2}{4}} \tag{44}$$

The result for the integration in Eq. (46) was obtained using Maple 7 software instead of applying the general formula provided by Gradshteyn and Ryzhik [25] for an indefinite integral involving the product of any two Bessel functions. It was found that the results from these two sources do not agree for all the cases involving a Bessel function and a modified Bessel function. In Eq. (41) is solved for $\overline{F}_{cm}$ by the method of the variation of parameters, yielding the following result.

$$\overline{F}_{cm} = \frac{\phi_{cm}}{2\beta}\left\{D_1 e^{\beta z}\left[\sqrt{2\pi}\left(1-\mathrm{erf}\left(\sqrt{2}u_1\right)\right) + (4u_1-2\beta)e^{-2u_1^2} + (\beta^2-4)\sqrt{\frac{\pi}{8}}\left(1-\mathrm{erf}\left(\sqrt{2}u_1\right)\right)\right]\right.$$
$$\left. + D_2 e^{-\beta z}\left[\sqrt{2\pi}\left(1+\mathrm{erf}\left(\sqrt{2}u_2\right)\right) + (4u_1+2\beta)e^{-2u_2^2} + (\beta^2-4)\sqrt{\frac{\pi}{8}}\left(1+\mathrm{erf}\left(\sqrt{2}u_2\right)\right)\right]\right\} \tag{45}$$

where

$$\beta = \pm\frac{1}{a_z}\left(\lambda_n^2 - \frac{Pe^2}{4}\right)^{\frac{1}{2}},$$
$$\phi_{cm} = \frac{\partial^2 g_{cm}}{\partial z^2}\int_0^1 r J_m(\lambda_n r) I_m\left(\frac{Pe}{2}r\right)\, dr,$$
$$D_1 = e^{2\left(\frac{Pe}{8a_z}+\frac{\beta}{4}\right)^2}, \qquad D_2 = e^{2\left(\frac{Pe}{8a_z}-\frac{\beta}{4}\right)^2},$$
$$u_1 = z + \frac{Pe}{8a_z} + \frac{\beta}{4}, \qquad u_2 = z + \frac{Pe}{8a_z} - \frac{\beta}{4},$$

$F_{cm}(r,m,z)$ is determined from $\overline{F}_{cm}(\lambda_n, m, z)$ by substituting Eq. (44) into the following inverse Hankel transform [24].

$$F_{cm}(r,m,z) = \sum_{n=1}^{\infty}\frac{J_m(\lambda_n r)}{N_r(\lambda_n)\bar{F}_{cm}(\lambda_n,m,z)} \tag{46}$$

where

$$N_r(\lambda_n) = \frac{J_m^2(\lambda_n)\left[\left(Bi^2+\lambda_n^2\right)-m^2\right]}{2\lambda_n^2}$$

The procedure for determining $F_{cm}(r,m,z)$ can be applied to obtain an expression for $F_{sm}(r,m,z)$, and then Eqs. (39), (40), (34), (22), (17) and (9) are used to determine the temperature distribution as given below:

$$T'(r,\theta,z) = T_\infty + T_m e^{bz}\left\{\sum_{m=0}^{\infty} cos(m\theta)\left[\sum_{n=1}^{\infty}\frac{J_m(\lambda_n r)\bar{F}_{cm}(\lambda_n,m,z)}{N_r(\lambda_n)} + f_{cm}(r,m)g_{cm}(z,m)\right]\right. \tag{47}$$
$$\left. + \sum_{m=1}^{\infty} sin(m\theta)\left[\sum_{n=1}^{\infty}\frac{J_m(\lambda_n r)\bar{F}_{sm}(\lambda_n,m,z)}{N_r(\lambda_n)} + f_{sm}(r,m)g_{sm}(z,m)\right]\right.$$

where

$$f_{sm} = C_1 I_m\left(\frac{Pe}{2}r\right)$$

$$g_{sm} = \frac{P_a S_{sm}}{N_\theta C_1\left[(m+Bi)I_m\left(\frac{Pe}{2}\right)+\frac{Pe}{2}I_m\left(\frac{Pe}{2}\right)\right]} e^{-\frac{Pe}{2a_z}z} e^{-2z^2}$$

Results and Discussion

Three-dimensional temperature profiles are determined using Eq. (47) due to laser heating of thin wires. A biocompatible material, MP35N, is chosen in this study because thin wires of this material are currently used to construct pacemaker leads, and the lead tip heats due to the radiofrequency magnetic field during magnetic resonance imaging. Currently, the leads are designed in a special way as resonant circuits to reduce heating. Each strand of the lead assembly, however, can be modified by a laser diffusion process to reduce heating. Typical thermophysical properties of MP35N used for calculating the temperature distribution are [15], density $\rho = 8430$ kg/m^3, thermal conductivity $k =$ 11.5 W/m K, specific heat capacity at constant pressure $c_p = 502$ J/kg K and melting temperature $T_m = 1315$ °C. The laser processing parameters are: laser power $P_i = 6$ W and the waist dimensions of the laser beam are $w_{x'} = 50$ and $w_{z'} = 500$ μm in the x′ and z′ directions, respectively, wire speed $U = 4$ mm/s and room temperature $T_\infty = 20$ °C.

Figure 3a–e are polar contour plots showing the temperature profiles at different cross sections starting from $z' = -0.5$ to $z' = 0.5$ mm that correspond to the axial locations beneath the laser beam. $z' = -0.5$ mm represents the cross section of the wire at an axial location 0.5 mm behind the laser beam center before entering into the laser spot, and $z' = 0.5$ mm represents the cross section of the wire at an axial location 0.5 mm in front of the laser beam center after passing through the laser spot. Each polar contour plot shows the temperature variation within the wire cross section. The upper half of the wire at a given cross section is heated since the laser beam is irradiated on the upper semicircle of the wire, while the lower half of the wire is heated due to the conduction of heat from the upper half and also cooled down due to convection. Starting at Fig. 3(a), one can see the effect of this laser direct heating and the conduction heating with simultaneous convection cooling on the temperature profiles. While the temperature is symmetric about $\theta = \pi/2$ and $\theta = 3\pi/2$ directions, it is asymmetric about $\theta = 0$ and $\theta = \pi$ directions due to the asymmetric heating mechanisms.

Figure 3(a–e) also show that the temperature distribution in the axial direction is asymmetric about $z' = 0$ axis (Fig. 1). Figure 3(b) and (e) are each 0.5 mm away from the laser beam center, i.e., the $z' = 0$ axis, but show two different temperature profiles in the azimuthal planes, and similarly Fig. 3(c) and (d), each of which is 0.25 mm away from the laser beam center, exhibit asymmetric temperature profiles. The temperatures are much higher in the positive axial direction than in the negative direction, which can be explained by the fact that the wire moves in the positive z′ direction and the laser

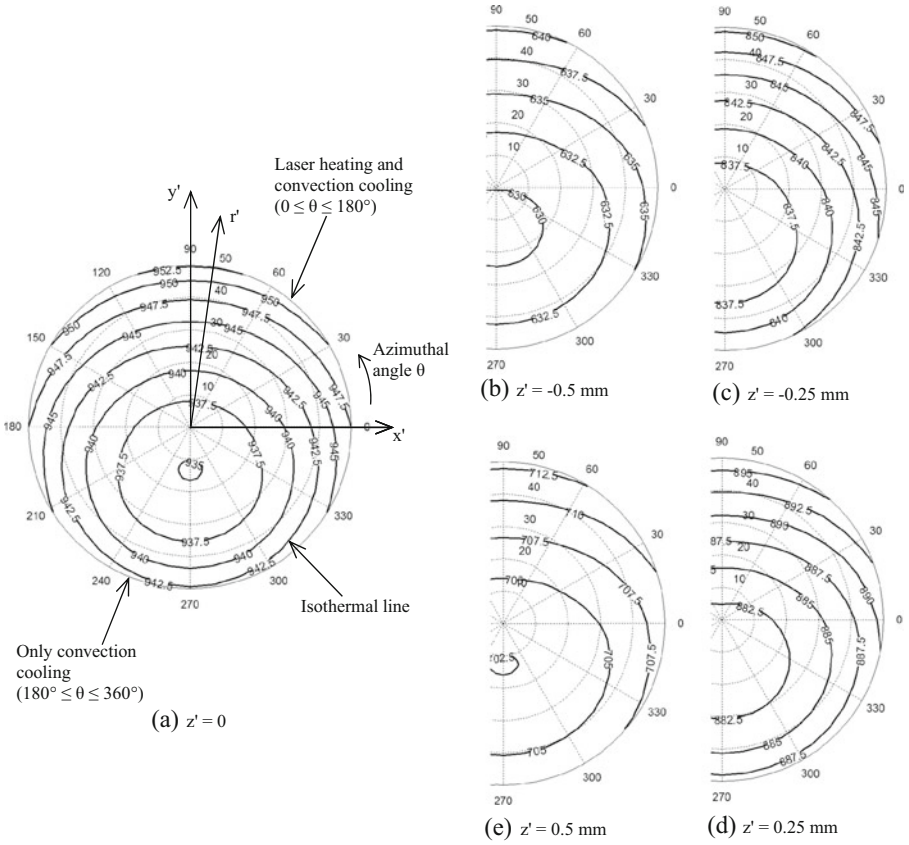

Fig. 3 Temperature distribution of wire cross section at different positions along the axis for Bi = 0.0011 and $h = 250$ W/m^2 K (Created using MS Word)

heating begins in negative z′. This heating process continues as the wire approaches toward the $z' = 0$ line where the laser irradiation is maximum. After the $z' = 0$ line, the laser heating mechanism is reduced because the laser irradiation decreases. There is, however, another heating mechanism, advection heating, due to the motion of the wire. Since the wire moves in the positive z′ direction, its temperature continues to rise to a maximum value a little after the $z' = 0$ line, which is discussed later, and then begins to decrease because of the reduction in both heating mechanisms. It is clear from Fig. 3 that the temperature distribution is neither axi-symmetirc nor uniform at a cross-section of the wire for Bi = 0.0011. The temperature across a solid is, generally, considered uniform if Bi < 0.1. Although Bi = 0.0011 satisfies the Biot number criterion of uniform temperature, the cross-sectional temperature of the wire is non-uniform in this study. It is, therefore, evident that the thermal response of the wire to rapid heating and cooling inherent in laser processing is different from the conventional heat conduction process, and this deviation can be attributed to the motion of the wire.

The effect of Bi is studied in Figs. 4 and 5 for Bi = 0.0027 and 0.0054 corresponding to the convection heat transfer coefficients 621 and 1242 W/m^2 K, respectively. The results in Figs. 3, 4 and 5 are obtained for the same parameters except the convection heat transfer coefficient. It can be seen from the isotherms at a given cross-section of

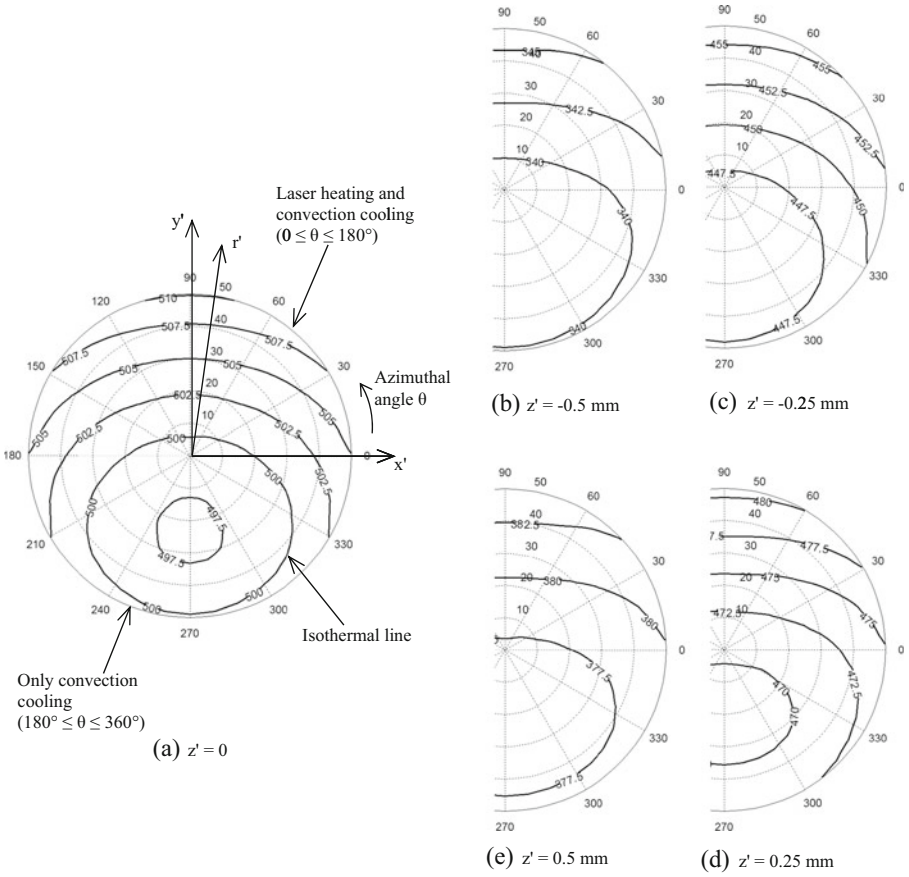

Fig. 4 Temperature distribution of wire cross section at different positions along the axis for Bi = 0.0027 and $h = 621$ W/m^2 K (Created using MS Word)

fixed axial position z′ in these figures that the temperature decreases as Bi increases, and also the difference between the maximum and minimum temperatures decreases as Bi increases. The temperature profiles are distorted more at high Bi than at low Bi. Figure 5(b) and (e) exhibit highly distorted temperature profiles due to high Bi of 0.0054. The lower value of Bi in Fig. 4, however, shows relatively less distortion in the temperature profile with fairly uniform temperature at a cross-section, which suggests that the limiting value of the Biot number to achieve uniform cross-sectional heating is much lower than the conventional limit of Bi as 0.1.

The minimum temperature at a particular cross-section of the wire does not occur at the center of the wire, instead it occurs at a point below the center of the cross-section. The effect of Bi on this trend is not evident at a low value of Bi as in Fig. 2, but can be clearly seen for a higher value of Bi as in Fig. 5. This effect is important particularly in laser-assisted diffusion process for determining whether the distribution of diffused atoms would be uniform along the entire circumference of the wire, because the diffusion coefficient and the generation of diffusant atoms by thermal decomposition of metallorganic compounds depend on temperature. Since the top half-surface of the wire is heated by the laser beam and the bottom half-surface is exposed to convection

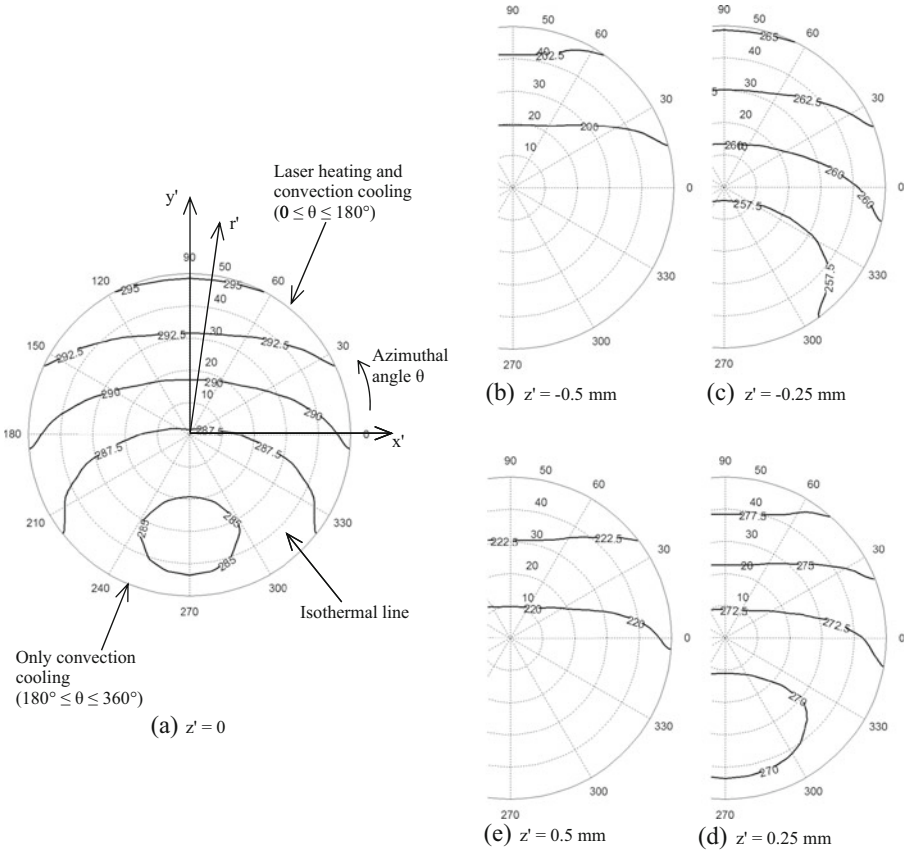

Fig. 5 Temperature distribution of wire cross section at different positions along the axis for Bi = 0.0054 and $h = 1242$ W/m^2 K (Created using MS Word)

cooling by the ambient gas, the temperature inside the bottom section rises due to heat conduction from the top to the bottom half of the wire. Therefore, depending on the Bi number, laser irradiance and thermal diffusivity, the laser-wire interaction time $\tau = \frac{2w_{z'}}{U}$ should be large to allow sufficient time for heat conduction to obtain uniform temperature distribution at least over a certain depth up to which the atoms have to be diffused. This mechanism will enable achieving uniform concentration of the diffused atoms in the azimuthal direction.

The radial variation of the temperature is plotted is Fig. 6 for various azimuthal angles, θ, on the cross-sectional plane $z' = 0$ to understand heat conduction inside the wire. The results in this figure show that Fig. 6 gives an idea of how much variation occurs in the surface temperature gradient. The direction of the laser beam has a higher temperature gradient between the centre of the wire and the surface while the opposite direction shows a lower temperature gradient. At $\theta = \pi/2$, which represents the positive y direction in the top half of the wire, the temperature increases radially from the center to the wire surface, while the temperature along the $\theta = 3\pi/2$ direction, which represents the negative y direction in the bottom half of the wire, the temperature decreases radially from the center and then begins to increase toward the wire surface. So the

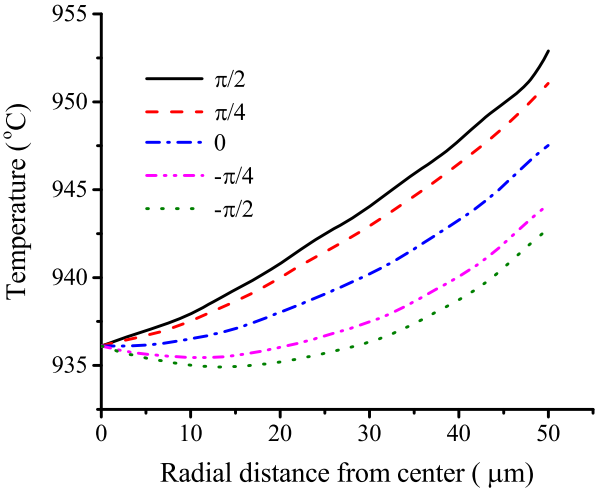

Fig. 6 Temperature distribution along radial direction at different angles for Bi = 0.0011 and $h = 250$ W/m^2 K (color only in online version - Created using Origin 9.1)

minimum temperature occurs off-center in the lower section of the wire, indicating that the heat flows from the wire surface toward an off-center point inside the wire. At the bottom half of the wire, the surface temperature is higher than the interior temperature even though the bottom surface is cooled by convection, which suggests that heat conduction from the top to the bottom section occurs dominantly in the azimuthal direction compared to the radial direction near the subsurface region of the wire.

The axial variation of the wire surface temperature due to localized heating by the laser beam is examined in Fig. 7, which shows that the rise in the temperature is limited to a very short length of the wire. Although the length of the heated region is about 2 mm, the temperature increases significantly over a shorter distance that approximately corresponds to the length of the laser beam on the surface of the wire. While moving

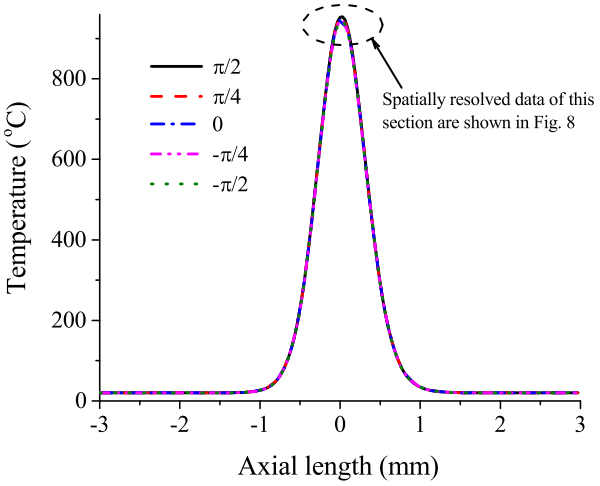

Fig. 7 Temperature distribution on the wire surface ($r = 1$) along axial direction at different angles for Bi = 0.0011 and $h = 250$ W/m^2 K (color only in online version - Created using Origin 9.1)

under the laser beam, the temperature increases as the wire approaches the laser beam center ($z' = 0$ mm) and then the temperature decreases as the wire travels away from the location of maximum temperature, indicating that the wire experiences heating and cooling cycles. Since the variation of temperature at different angles cannot be seen clearly in Fig. 7, spatially-resolved temperatures of the region around $z' = 0$ are plotted in Fig. 8 for different angles. As discussed earlier, the maximum temperature occurs slightly after $z' = 0$ due to the motion of the wire in the z′ direction. For a given velocity of the wire, however, Fig. 8 shows that the location of maximum temperature does not shift significantly from $z' = 0$ toward the z′ direction for small values of Bi such as Bi = 0.0011. Small values of Bi, therefore, reduce the effect of wire speed on shifting the maximum temperature away from the laser beam center. However, higher speed of the wire with a higher Peclet number, which is defined as the ratio of the advective heat transfer rate to the conductive heat transfer rate, shifts the position of the maximum temperature further down the z′ direction from the laser beam center. This effect of shifting the maximum temperature is particularly important for modifying the property of the wire surface at micro- and nano-scales. Figure 8 also shows that the maximum temperatures occur at the same value of z′, i.e., $z' = 0.0176$ mm, for all values of θ, indicating that the maximum temperatures lie on the same cross-sectional plane. Although the temperature varies in the axial direction for each angle, the trend of this variation is similar for all the angles.

At a particular angle $\theta = \pi/2$, the axial temperature distribution is presented in Fig. 9 for different radii to analyze the heating process inside the wire. These results, which are similar to those in Fig. 7, show that the laser heating is localized over a short length inside the wire and the interior points also experience rapid heating and cooling cycles. Since Fig. 9 does not clearly show the different values of temperature at different radial points, the temperatures of the region around $z' = 0$ are plotted in Fig. 10 for various radii. Figure 10 exhibits the same trend in the temperature distribution as in Fig. 8, i.e., the maximum temperatures at various radial points occur slightly after the laser beam

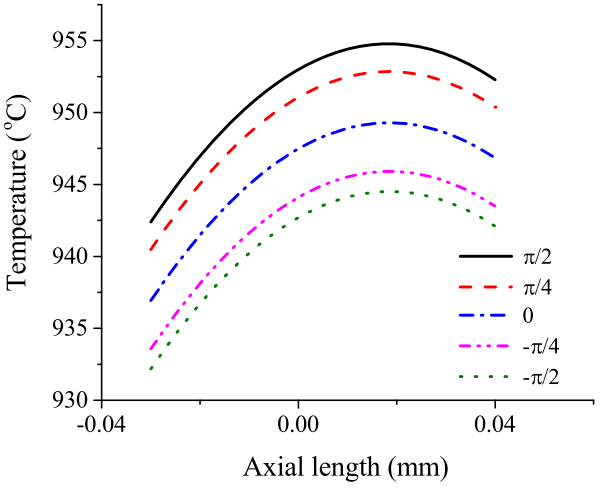

Fig. 8 Maximum temperature on the wire surface ($r = 1$) at different angles for Bi = 0.0011 and $h = 250$ W/m^2 K (color only in online version - Created using Origin 9.1)

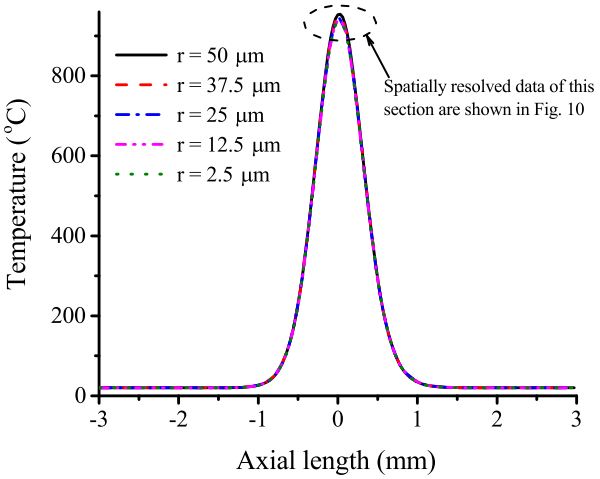

Fig. 9 Temperature distribution at laser direction $\theta = \pi/2$ along axial direction at different radius for Bi = 0.0011 and $h = 250$ W/m^2 K (color only in online version - Created using Origin 9.1)

center ($z' = 0$). Also the maximum temperatures lie on the same cross-sectional plane because they occur at the same value of z′, i.e., $z' = 17.6$ μm, for all values of r′.

Conclusions

An analytic solution is obtained for the three-dimensional quasi-steady state temperature distribution during laser heating of long moving cylinders. This analysis is applied to wires of small (100 μm) diameter and the temperature distribution is found to depend on the axial as well as radial positions and the azimuthal angle. The temperature across the cross-section is found to be non-uniform for Bi numbers much lower than the conventional Bi number criterion for uniform temperature (Bi < 0.1). On a given cross-sectional plane, the minimum temperature occurs below the center of the wire and the

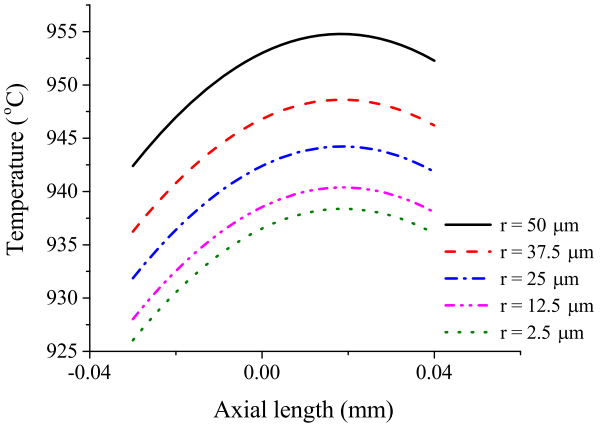

Fig. 10 Maximum temperature at laser direction $\theta = \pi/2$ at different radius for Bi = 0.0011 and $h = 250$ W/m^2 K (color only in online version - Created using Origin 9.1)

temperature profiles of the upper and lower halves of the wire are asymmetric, indicating that the temperature distribution is not axisymmetric. The temperature over a certain depth in the circumferential region is higher than the interior temperature on a cross-sectional plane, which suggests that the azimuthal heat conduction is dominant near the surface compared to the radial conduction. The laser heating region in the axial direction is limited to a very narrow length, which is approximately equal to the length of the laser beam on the wire surface, and the wire experiences rapid heating and cooling as it approaches the beam center and moves away from the location of maximum temperature, respectively. The maximum temperature is shifted from the laser beam center toward the z direction depending on the Bi number, and the velocity of the wire or the Pe number. Small values of Bi and Pe reduce the shift, yielding the maximum temperature very close to the beam center. The shift in the maximum temperature occurs at the wire surface as well as inside the wire for all azimuthal angles and radial points, and these maximum temperatures lie on the same cross-sectional plane.

References

1. Chen, S.-Y., Benafan, O., Vaidyanathan, R., Kar, A.: Laser polarization-assisted diffusion for modifying electromagnetic properties of metals. Opt. Lasers Eng. **62**, 132–138 (2014)
2. Chen, S.-Y., Benafan, O., Vaidyanathan, R., Kar, A.: Modulation of diffusion with polarized lasers. Appl. Phys. A Mater. Sci. Process. **116**, 703–713 (2014)
3. Benafan, O., Chen, S-Y., Marshell, M.T., Kar, A., Vaidyanathan, R.: Laser surface modification of medical grade alloys for reduced heating in an MRI environment. *Progress in Electromagnetics Research Symposium,* Marrakesh, Morocco, 20–23 March, 2011
4. Steen, W.M., Mazumder, J.: Laser Material Processing. Springer, London (2010)
5. John, D.: Mathematics in laser processing. In: John, D. (ed.) The Theory of Laser Material Processing Heat and Mass Transfer in Modern Technology, pp. 1–18. Springer, Netherlands (2009)
6. Gross, M.: Comprehensive numerical simulation of laser materials processing. In: John, D. (ed.) The Theory of Laser Material Processing Heat and Mass Transfer in Modern Technology, pp. 339–356. Springer, Netherlands (2009)
7. Zill, D.G., Wright, W.S.: Advanced Engineering Mathematics Fourth Edition. Jones & Bartlett Publishers, Sudbury (2010)
8. Yilbas, B.S.: Laser Heating Applications Analytical Modelling. Elsevier, New York (2012)
9. Grigorenko, A.N., Panina, L.V., Sandacci, S.I., Makhnovskiy, D.P., Mapps, D.J., Khrushchev, I.Y., Dubov, M.V., Larin, V., Torkunov, A.: Laser processing effect on magnetic properties of amorphous wires. Appl. Phys. Lett. **81**, 4790–4792 (2002)
10. Madic, M.J., Radovanovic, M.R.: Analysis of the heat affected zone in CO_2 laser cutting of stainless steel. Therm. Sci. **16**, S363–S373 (2012)
11. Yilbas, B.S., Al-Dweik, A.Y.: Analytical solution to laser short-pulse heating of microsized metal wire: volumetric and surface heat source considerations. Can. J. Phys. **90**, 911–918 (2012)
12. Yilbas, B.S., Sami, M., AbuAlHamayel, H.I.: 3-dimensional modelling of laser repetitive pulse heating: a phase change and moving heat source considerations. Appl. Surf. Sci. **134**, 159–178 (1998)
13. Gospavic, R., Sreckovic, M., Popov, V., Todorovic, G.: 3D modelling of material heating with laser beam for cylindrical geometry. Math. Comput. Model. **43**, 620–631 (2006)
14. Mazhukin, V.I., Nosov, V.V.: Mathematical modelling of nonequlibrium heating and melting of Si by Nd-YAG laser radiation at radiation wavelength 1.06 μm 1995: Proceedings of the 5th International Conference on Industrial Lasers and Laser Applications '95, Shatura, Moscow Region, Russia, 24-26 June 1995, In: Panchenko, V. Ya., Golubev, V. S. (eds.) SPIE, pp. 236–247. Bellingham, WA (1996)
15. Carpenter Technology Corporation.: Alloy Data Capenter® MP35N Alloy. CRC Holdings, Fort Worth, TX. http://www.veridiam.com/pdf/DataSheetMP35NAlloy.pdf (2003). Accessed 03 November 2015
16. Incropera, F.P., Dewitt, D.P., Bergman, T.L., Lavine, A.S.: Fundamentals of Heat and Mass Transfer, 6th edn, pp. 8–261. Wiley, New York (2007)

17. Sano, Y., Mukai, N., Olazaki, K., Obata, M.: Residual stress improvement in metal surface by underwater laser irradiation. Nucl. Instrum. Methods B **121**, 432–436 (1997)
18. Jin, B., Li, M., Hawang, T.W., Moon, Y.H.: Feasibility studies on underwater laser surface hardening process. Adv. Mater. Sci. Eng. (2015). doi:10.1155/2015/845273
19. Kruusing, A.: Underwater and water-assisted laser processing: part 1—general features, steam cleaning and shock processing. Opt. Lasers Eng. **41**, 307–327 (2004)
20. Kruusing, A.: Underwater and water-assisted laser processing: part 2—etching, cutting and rarely used methods. Opt. Lasers Eng. **41**, 329–352 (2004)
21. Ready, J.F.: Effects of High-Power Laser Radiation, p. 72. Academic, New York (1971)
22. Brown, M.S., Arnold, C.B.: Fundamentals of laser-material interaction and application to multiscale surface modification. In: Sugioka, K., Michel, M., Piqué, A. (eds.) Laser Precision Microfabrication, p. 94. Springer, New York (2010)
23. Oliver, F.W.J.: Bessel functions of integer order. In: Abramowitz, M., Stegun, I.A. (eds.) Handbook of Mathematical Functions with Formulas Graphs and Mathematical Tables, p. 376. Dover Publications, New York (1972)
24. Özişik, M.N.: Heat Conduction, 2nd edn, pp. 99–109 & 528–545. Wiley, New York (1993).
25. Gradshteyn, I. S., Ryzhik, I. M.: Tables of Integral, Series, and Products 7th Ed. Jeffrey, A., Zwillinger, D. (eds.) Elsevier Academic Press, USA, (2007)